

Entanglement Wedge Minimum Cross-Section in Holographic Axion Gravity Theories

Fang-Jing Cheng ^{1,*} Zhe Yang ^{1,†} Chao Niu ^{1,‡} Cheng-Yong Zhang ^{1,§} and Peng Liu ^{1,¶}

¹ *Department of Physics and Siyuan Laboratory,
Jinan University, Guangzhou 510632, China*

Abstract

We study the mixed state entanglement properties in two holographic axion models by examining the behavior of the entanglement wedge minimum cross section (EWCS), and comparing it with the holographic entanglement entropy (HEE) and mutual information (MI). We find that the behavior of HEE, MI and EWCS with Hawking temperature is monotonic, while the behavior with the axion parameter k is more rich, which depends on the size of the configuration and the values of the other two parameters. Interestingly, the EWCS monotonically increases with the coupling constant κ between the axion field and the Maxwell field, while HEE and MI can be non-monotonic. It suggests that the EWCS, as a mixed state entanglement measure, captures distinct degrees of freedom from the HEE and MI indeed. We also provide analytical understandings for most of the numerical results.

*Electronic address: chengfj@stu2018.jnu.edu.cn

†Electronic address: yzar55@stu2021.jnu.edu.cn

‡Electronic address: niuchaophy@gmail.com

§Electronic address: zhangcy@email.jnu.edu.cn

¶Electronic address: phylp@email.jnu.edu.cn; corresponding author

Contents

I. Introduction	2
II. Information related quantities	4
A. Holographic entanglement entropy	4
B. Mutual information	6
C. Entanglement Wedge Minimum Cross Section	6
D. Classification of configuration	7
III. Model I	8
A. Background solution	8
B. Entanglement Wedge Minimum Cross Section	9
IV. Model II	11
A. Background solution	11
B. Holographic entanglement entropy	12
C. Mutual information	16
D. Entanglement Wedge Minimum Cross Section	17
V. Discussion	21
Acknowledgments	22
References	22

I. INTRODUCTION

In recent years, research on quantum entanglement has attracted more and more attention across many different fields, including quantum information, condensed matter physics and quantum gravity [1–4]. Many measures of quantum entanglement have been found to diagnose the quantum phase transition of strongly correlated systems, which opens a gate to the study of condensed matter physics from an information perspective. Furthermore, quantum entanglement is also considered crucial in the emergence of spacetime, which brings a new understanding for the essence of spacetime [5–11].

There are many measures of quantum entanglement, such as entanglement entropy (EE), mutual information (MI) and entanglement of purification (EoP). All of them can describe quantum entanglement to certain extent. The EE is only suitable for describing pure state entanglement. But most quantum systems are in mixed state in nature, so it is necessary to describe them with other measures, such as MI and EoP, which can extract the quantum as well as classical correlations from the mixed state systems. However, the entanglement measures are notoriously difficult to calculate, which has become the main obstacle in the study of quantum entanglement [12, 13].

Over the past two decades, holographic duality theory has been widely adopted in many fields of physics [14–17]. Recently, the measures of quantum entanglement of strongly correlated systems have been considered to be related to the geometric quantity of dual gravity systems, which provides a simple geometric method for calculating the quantum entanglement. It was first proposed that the holographic entanglement entropy (HEE), which is the holographic version of EE, is proportional to the area of the minimum surface in the dual gravity system [2], and has many applications in diagnosing the phase transitions [18–24]. After that, more holographic duality relations between the measures of quantum entanglement and the geometric quantity of dual gravity system have been proposed. For example, holographic Rényi entropy is proportional to the minimum area of cosmic branes [4]. Moreover, the butterfly effects and quantum complexity and many other measures have been proposed and studied in [25–45]. Entanglement of purification (EoP) and negativity has been associated with the minimum area of entanglement wedge minimum cross section (EWCS) in the dual gravity spacetime [46, 47]. Recently, our work proposed that EWCS can describe the thermal phase transitions of mixed state systems [48–51].

At present, HEE, as the earliest progress in the subject of holographic quantum information, has been widely studied. However, the studies on entanglement of mixed states such as MI and EWCS are still far from comprehensive. Holographic linear axion models are simple enough to have analytical solutions while having rich physical content, such as momentum dissipation, phonons, etc [52]. Therefore, in this paper, we will study the properties of mixed state entanglement in linear axion models in detail.

We organize this paper as follows: in Sect. II, we review the concepts of three entanglement measures (HEE, MI, EWCS) and the configurations we will study. In Sect. III, we discuss the properties of EWCS in the first linear axion model. In Sect. IV, we discuss the

properties of three entanglement measures (HEE, MI, EWCS) in the second linear axion model. Finally, we summarize in Sect. V.

II. INFORMATION RELATED QUANTITIES

In this section, we introduce the concepts and calculation methods of HEE, MI and EWCS.

A. Holographic entanglement entropy

HEE has been considered proportional to the area of the minimum surface extending into the bulk [2]. Although this duality is very concise, it is difficult to calculate. To simplify the calculation, we consider the infinite strip configuration along y -axis (see Fig. 1 (a)) in a homogeneous spacetime,

$$ds^2 = g_{tt}dt^2 + g_{xx}dx^2 + g_{yy}dy^2 + g_{zz}dz^2, \quad (1)$$

where $z = \frac{r_h}{r}$, which means that $z = 0$ is the AdS boundary and $z = 1$ the horizon of the black brane. This configuration is invariant along the y -axis, so its width w is enough to characterize it. The minimum surface can be parameterized as $z(x)$ on the $x - z$ plane. The area of the minimum surface is,

$$A = L_y \int \sqrt{g_{yy}(g_{xx}dx^2 + g_{zz}dz^2)} = L_y \int \sqrt{g_{yy}(g_{xx} + g_{zz}z'(x)^2)}dx = L_y \tilde{A} \propto \tilde{A}, \quad (2)$$

where $\tilde{A} = \int \sqrt{g_{yy}(g_{xx} + g_{zz}z'(x)^2)}dx$. $L_y = \int dy$ is the infinite length of the y -axis, which we ignore since it is a constant. Therefore, we only focus on \tilde{A} . Varying \tilde{A} leads to the equations of motion of the minimum surface. Due to the divergence of asymptotic AdS at $z = 0$, the parameterization $z(x)$ is not suitable for solving the minimum surface. A better candidate parameterization is the angle θ ,

$$\tilde{A} = \int \sqrt{g_{yy}(z(\theta))(g_{xx}(z(\theta))x'(\theta)^2 + g_{zz}(z(\theta))z'(\theta)^2)}d\theta, \quad (3)$$

with $\tan \theta = \frac{z}{x}$ [49, 50]. Also, the equations of motion for $z(\theta)$ and $x(\theta)$ can be obtained by varying \tilde{A} . Asymptotic AdS will lead to a divergent \tilde{A} . Therefore, in practical calculations,

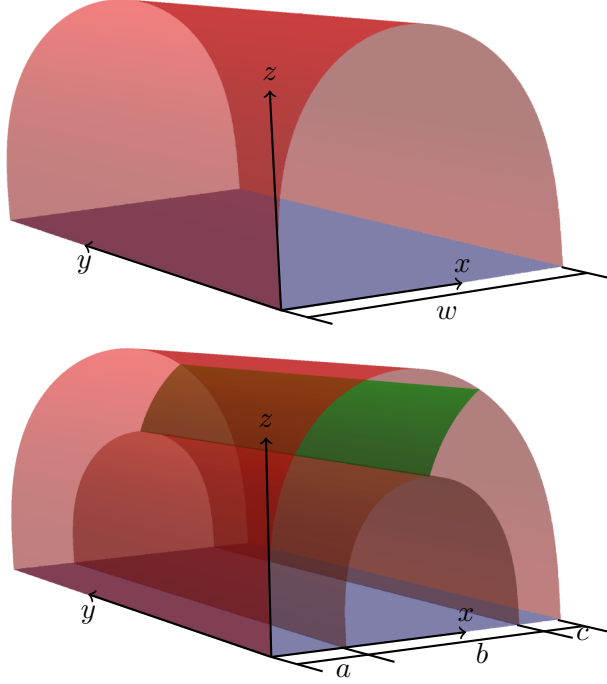


FIG. 1: A cartoon of the studied configuration. (a) The upper figure shows the configuration used to discuss HEE. (b) The lower figure shows the configuration used to discuss MI and EWCS.

we need to subtract a common divergent term \tilde{A}_{AdS} brought by the AdS. We treat the remaining finite term S as the EE,

$$S = \tilde{A} - \tilde{A}_{AdS}. \quad (4)$$

When the width of the configuration is very small, the minimum surface resides near the AdS boundary. Therefore, the HEE with small configuration is the same as that of AdS. However, when the configuration is large (i.e. the width w of the infinite strip is large), the minimum surface will be close to the horizon of the black brane. At this time, the HEE will be mainly contributed by the thermal entropy. The HEE will behave as

$$S \simeq sw, \quad (5)$$

where s is the thermal entropy density. In other words, HEE with large configurations is dictated by the thermal entropy, which may bury the real quantum entanglement. This is the understanding of the influence of thermal entropy contained in HEE from the perspective of holography [49].

B. Mutual information

The mutual information between two disjoint subsystems A and C separated by B (with widths a , b and c) is defined as

$$I(A; C) = S(A) + S(C) - S(A \cup C), \quad (6)$$

where $S(\#)$ is the entanglement entropy of the region $\#$. More specifically, the minimum surface for $A \cup C$ has two locally minimum candidates from which we choose the minimum as the right one,

$$S(A \cup C) = \min[S(A) + S(C), S(B) + S(A + B + C)]. \quad (7)$$

When $S(A \cup C) = S(A) + S(C)$, we have $I(A; C) = 0$. In this case, there is no entanglement between A and C systems, and MI is trivial. When $S(A \cup C) = S(B) + S(A + B + C)$, we have $I(A; C) > 0$. In this case, MI is nontrivial [53].

Obviously, the definition of MI is directly based on the definition of HEE. However, MI by definition cancels out the divergent term of HEE. In addition, MI partially offsets the influence of thermodynamic entropy [53]. This shows that MI is more suitable than HEE to measure the entanglement of mixed states.

C. Entanglement Wedge Minimum Cross Section

In addition to calculating the entanglement of the mixed state by directly subtracting the influence of the thermal entropy like MI, we can also purify the mixed state by introducing additional degrees of freedom, so as to extract the quantum entanglement. This is called the entanglement of purification (EoP) [12]. Specifically, the EoP is defined as the minimum entanglement entropy among all possible purification. Later, it was proposed that EoP is proportional to the minimum cross section in the entanglement wedge of the dual spacetime [46] (see the green section in Fig. 1 (b)),

$$E_W(\rho_{AB}) = \min_{\Sigma_{AB}} \left(\frac{Area(\Sigma_{AB})}{4G_N} \right). \quad (8)$$

In addition to EoP, the reflected entropy, negativity, etc [54, 55], are also proposed dual to EWCS. From the definition, EWCS is neither dominated by the AdS boundary nor

dominated by the near horizon geometry. Therefore, EWCS is not dictated by thermal entropy, and hence is free from the divergence problem caused by AdS.

The EWCS with symmetrical configuration ($a = c$) is obviously a vertical plane, so its calculation is very simple. However, it is very difficult to calculate EWCS for asymmetric configurations ($a \neq c$). In [49], we proposed a numerical algorithm to calculate EWCS using translation invariance. Later in [51], we proposed an improved algorithm based on Newton iteration, which greatly improves the accuracy of EWCS calculation.

D. Classification of configuration

To more clearly discuss the relationship between configuration and information related physical quantities, we divide configuration into three categories: large, intermediate and small configurations.

For HEE, we categorize configuration according to the behavior under the limit of width: if the behavior of HEE with parameters is the same as the case when the configuration width tends to zero, the corresponding configuration is small; if the behavior of HEE with parameters is the same as the case when the configuration width tends to infinity, the corresponding configuration is large; otherwise, the corresponding configuration is intermediate. The advantage of this classification is that the small configuration directly reflects the properties of the AdS boundary, and the large configuration directly reflects the properties of the thermal entropy. In addition, the behavior of HEE with parameters under intermediate configuration may be very complicated and need extra understandings.

For MI and EWCS, the configurations here involve the widths of A , B and C , so the classification of large, intermediate and small configurations in HEE case cannot be straightforwardly applied. We adopt the following conditions: if the minimum surface corresponding to $A \cup B \cup C$ is very close to the AdS boundary, then the corresponding configuration is small; if the minimum surface corresponding to A and C are all very close to the horizon of the black brane, then the corresponding configuration is large. In other cases, the corresponding configuration is intermediate.

Next, we discuss HEE, MI and EWCS on two different axion models.

III. MODEL I

A. Background solution

In the previous work [50], HEE, MI and EWCS of symmetric configuration in model I are discussed. This section will supplement the discussion of EWCS in model I with asymmetric configurations. The action of the model I is,

$$S = \int d^4x \sqrt{-g} \left[R + 6 - V(X) - \frac{1}{4} F_{\mu\nu} F^{\mu\nu} \right], \quad (9)$$

where $V(X)$ is the kinematic term of the axion fields ψ^I . Ansatz and the corresponding solutions are,

$$\begin{aligned} ds^2 &= -f(r)dt^2 + \frac{1}{f(r)}dr^2 + r^2\delta_{ij}dx^i dx^j, \\ A_t &= \mu - \frac{\rho}{r}, \quad \psi^I = k\delta_i^I x^i, \\ X &= \frac{1}{2}g^{ab}\delta_{IJ}\partial_a\psi^I\partial_b\psi^J, \quad \text{where } i, j, I, J = 1, 2, \end{aligned} \quad (10)$$

with

$$f(r) = \frac{\rho^2}{4r} \left(\frac{1}{r} - \frac{1}{r_h} \right) + \frac{1}{2r} \int_{r_h}^r \left[6u^2 - V\left(\frac{k^2}{u^2}\right) u^2 \right] du. \quad (11)$$

The ψ^I represents the linear axion field with a constant linear factor k . The vector field A is the Maxwell field, and μ, ρ represent the chemical potential and the charge density of the dual field theory. For regularity, the value of the Maxwell field on the horizon vanishes, thus we have $\rho = \mu r_h$.

For simplicity, we choose $V(X) = X^2$. The system (10) is invariant under the following rescaling,

$$\begin{aligned} (t, x, y) &\rightarrow \alpha(t, x, y), \\ (r, k, \mu) &\rightarrow (r, k, \mu)/\alpha, \\ (f(r), \rho) &\rightarrow (f(r), \rho)/\alpha^2. \end{aligned} \quad (12)$$

We focus on scaling-invariant physical quantities, so we adopt μ as the scaling unit by setting $\mu = 1$. Hawking temperature is given by,

$$T = \frac{f'(r)}{4\pi} \Big|_{r=r_h} = -\frac{r_h^2 + 2k^4 - 12r_h^4}{16\pi r_h^3}. \quad (13)$$

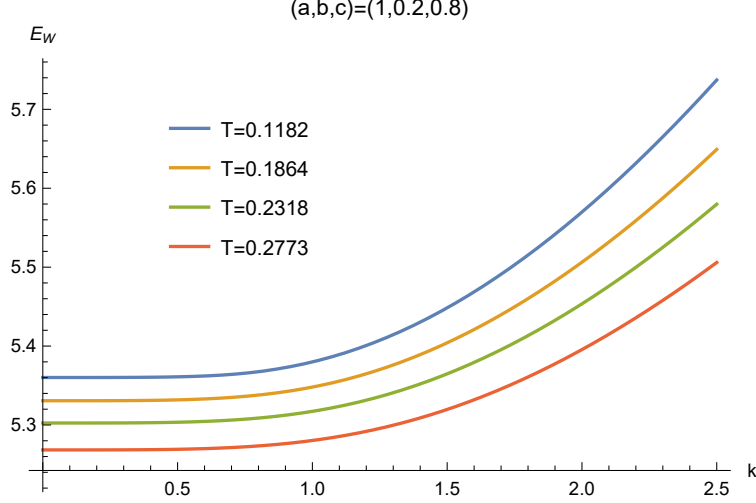


FIG. 2: The relation between EWCS and k in the large configuration for model I. It can be seen from the figure that EWCS increases monotonically with k , and it also has the same monotonic behavior under other large configurations and T .

B. Entanglement Wedge Minimum Cross Section

We find that the behavior of EWCS with k depends on the details of the configurations and the value of T . In large configurations, the EWCS increases monotonically with k , independent of the value of T . We show this phenomenon in Fig. 2. Moreover, when k is small, the slope is very small.

In small configurations, when the value of T is appropriate, the non-monotonic behavior of EWCS with k will appear, as shown in Fig. 3. Specifically, the EWCS decreases first and then increases with k . We also find that the minimum point will shift to the left with the increase of temperature, and the decreasing behavior of EWCS with k will weaken or even disappear when the configuration is fixed. These conclusions can be more easily drawn from Fig. 4.

Moreover, we find that EWCS decreases monotonically with T , but is independent of configuration and k (see Fig. 5). The behavior that EWCS decreases with T can be understood from the perspective of dual physics. Increasing the temperature of the quantum system can destroy the entanglement between subregions, so the physical quantities related to the entanglement of mixed states should decrease with the increase of temperature.

Next, we discuss the relationship between the EWCS of asymmetric configuration dis-

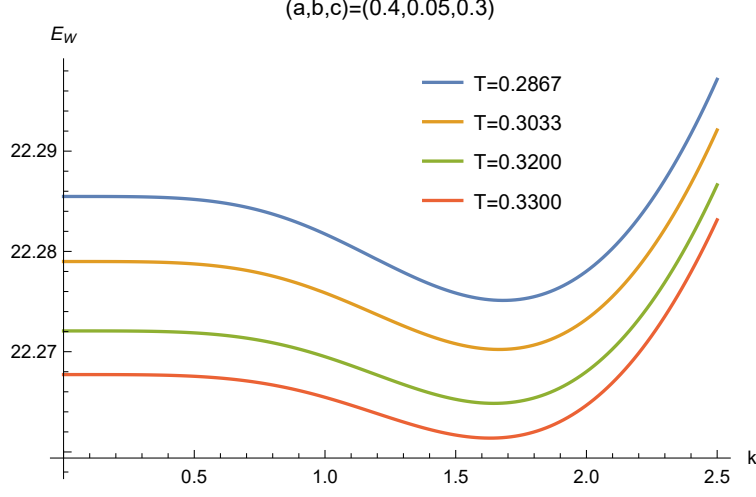


FIG. 3: The relation between EWCS and k in the small configuration for model I. It can be seen that when T is appropriate, EWCS first decreases and then increases with k .

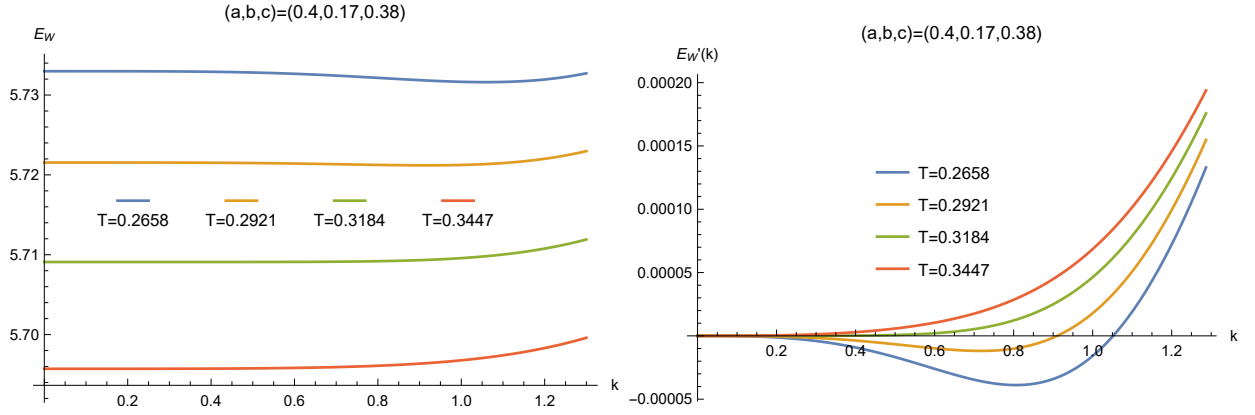


FIG. 4: The figure on the left shows the relation between EWCS and k in another small configuration for model I. The figure on the right shows the relation between the derivative of EWCS to k and k for model I. It can be seen from the figure on the left that the decreasing behavior of EWCS with k weakens or even disappears when the temperature increases. This conclusion can be seen more clearly in the figure on the right. Moreover, we can see from the right figure that when EWCS is non-monotonic with k , the increase of T will make the minimum point shift to the left.

cussed here and the EWCS of symmetric configuration have discussed in [50]. First, the relationship between EWCS and temperature is the same in both cases, which is also in line with the physical expectation that high temperature breaks the entanglement. However, the EWCS with asymmetric configuration can exhibit non-monotonic behavior with k .

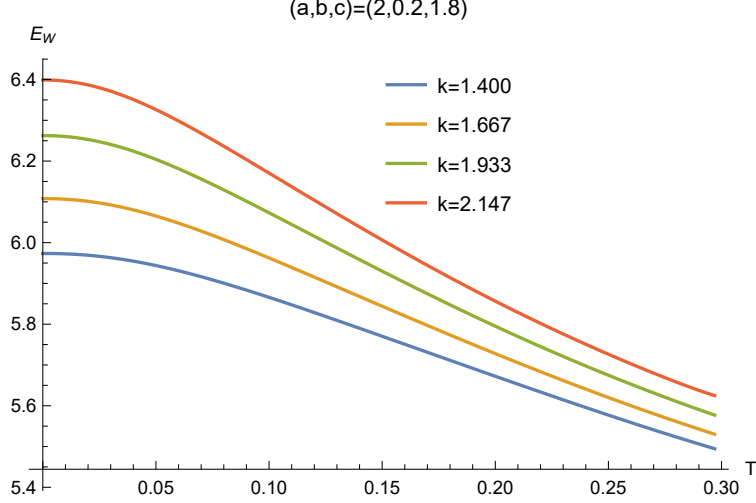


FIG. 5: The relation between EWCS and T for model I. It can be seen from the figure that EWCS decreases monotonically with T , and it also has the same monotonic behavior under other configurations and parameters.

This shows that asymmetric configurations can capture more information than symmetric configurations, which is also one of our main motives to study asymmetric configuration.

IV. MODEL II

A. Background solution

The action for model II is [52, 56, 57],

$$S = \int d^4x \sqrt{-g} \left[R + 6 - V(X) - \frac{1}{4} (1 + \kappa \text{Tr}[X]) F_{\mu\nu} F^{\mu\nu} \right], \quad (14)$$

where $V(X)$ is the kinematic term of the axion fields, κ represents the coupling constant between the axion and the Maxwell field. The ansatz and the background solutions are,

$$ds^2 = -f(r)dt^2 + \frac{1}{f(r)}dr^2 + r^2\delta_{ij}dx^i dx^j, \quad (15)$$

$$A_t = \mu - \frac{\pi\rho}{2k\sqrt{|\kappa|}} + \rho \frac{{}_2F_1(1, -\frac{1}{2}; \frac{1}{2}; -\frac{r^2}{\kappa k^2}) - 1}{r}, \quad \psi^I = k\delta_i^I x^i, \quad (16)$$

$$X = \frac{1}{2}g^{ab}\delta_{IJ}\partial_a\psi^I\partial_b\psi^J, \quad \text{where } i, j, I, J = 1, 2, \quad (17)$$

with

$$f(r) = \frac{1}{2r} \int_{r_h}^r \left[\left(6 - V\left(\frac{k^2}{s^2}\right) \right) s^2 - \frac{1}{2} \frac{\rho^2}{s^2 + \kappa k^2} \right] ds. \quad (18)$$

The ψ^I represents the linear axion field with a constant linear factor k . Like model I, The vector field A is the Maxwell field, and μ, ρ represent the chemical potential and the charge density of the dual field theory. The coupling $\kappa \text{Tr}[X] F_{\mu\nu} F^{\mu\nu}/4$ between the axion field and the Maxwell is the main difference between the present model II and model I. When $\kappa = 0$, model II will return to model I. Therefore, we will focus on the influence of this coupling term on the physical quantities related to quantum information.

Again, we specifically choose $V(X) = X^2$ for concreteness. The regularity condition for the Maxwell field on the horizon is,

$$\mu - \frac{\pi\rho}{2k\sqrt{|\kappa|}} + \rho \frac{{}_2F_1(1, -\frac{1}{2}; \frac{1}{2}; -\frac{r_h^2}{\kappa k^2}) - 1}{r_h} = 0. \quad (19)$$

The setup of this model is invariant under the following rescaling,

$$\begin{aligned} (t, x, y) &\rightarrow \alpha(t, x, y), \\ (r, k, \mu) &\rightarrow (r, k, \mu)/\alpha, \\ (f(r), \rho) &\rightarrow (f(r), \rho)/\alpha^2. \end{aligned} \quad (20)$$

We focus on scaling-invariant physical quantities, so again we adopt μ as the scaling unit by setting $\mu = 1$. Hawking temperature is given by,

$$T = \frac{1}{16\pi} \left[2r_h \left(6 - V\left(\frac{k^2}{r_h^2}\right) \right) - \frac{\rho^2}{r_h^3(1 + \kappa(k^2/r_h^2))} \right]. \quad (21)$$

In addition, we find that when $\kappa < 0$, the black brane solution can be complex in certain regions of the bulk. Therefore, throughout this paper only we discuss the case of $\kappa \geq 0$.

B. Holographic entanglement entropy

In this subsection, we explore the relationship between HEE and system parameters (k, T, κ) in model II.

First, we study HEE vs k . We find that HEE increases monotonically with k when κ is relatively small. This can be deduced from the relationship between the r_h and k at relatively small values of κ . From the Hawking temperature (21) and the horizon condition (19), we can deduce that,

$$T = - \frac{\frac{2\kappa k^2}{(\kappa k^2 r_h + r_h^3)(\pi - 2 \arctan(\frac{r_h}{\sqrt{\kappa} k})^2) + \frac{k^4}{r_h^3} - 6r_h}}{8\pi}. \quad (22)$$

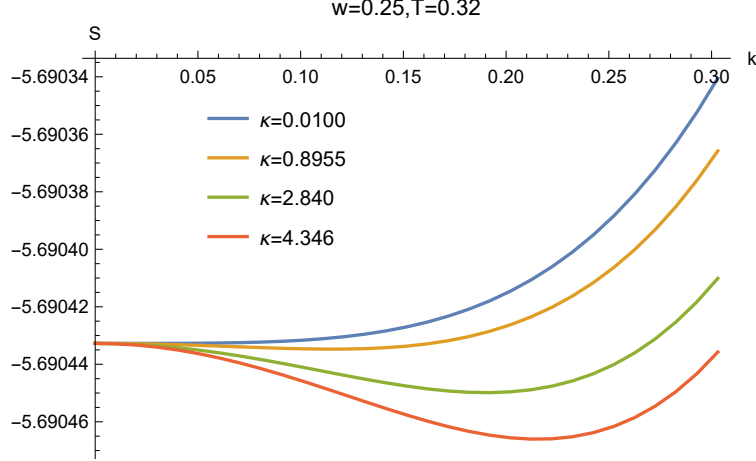


FIG. 6: The relation between HEE and k in the small configuration for model II. It can be seen that when κ is very small, HEE increases monotonically with k , and with the increase of κ , the behavior of HEE decreases first and then increases with k .

Taking $\kappa \rightarrow 0$ limit, one obtain that,

$$T = \frac{6r_h^4 - k^4}{8\pi r_h^3}. \quad (23)$$

Therefore, one find that,

$$\partial_k r_h = \frac{4k^3 r_h}{3(2r_h^4 + k^4)} > 0. \quad (24)$$

The relationship (24) suggests that r_h monotonically increases with k when κ is small. The increasing r_h means that the horizon moves closer to the boundary, and the minimum surface will stretch to the near-horizon region, and be affected by the thermal entropy. The fact that r_h increases with k also suggests that the thermal entropy increases with k . When κ further increases, HEE decreases first and then increases with k . We show this result in Fig. 6. The monotonically increasing behavior between the HEE and k when k is large enough cannot be analyzed by taking $\kappa \rightarrow 0$. Instead, when k is relatively large, it is readily seen that ${}_2F_1\left(-\frac{1}{2}, 1; \frac{1}{2}; -\frac{r_h^2}{\kappa k^2}\right)$ will be small, then one can expand it as,

$$\begin{aligned} \partial_k r_h &= \frac{4kr_h (2\pi^3 \kappa k^4 r_h^2 + \pi^3 k^2 r_h^4 - 2\kappa^{3/2} k r_h^3 + \pi \kappa r_h^4 + \pi^3 \kappa^2 k^6)}{2\kappa k^2 r_h^2 (-4\sqrt{\kappa} k r_h + 3\pi r_h^2 + \pi \kappa k^2) + 3\pi^3 (2r_h^4 + k^4) (r_h^2 + \kappa k^2)^2} \\ &= \frac{4r_h}{3k} + O(k^{-2}) > 0. \end{aligned} \quad (25)$$

Therefore, when k is relatively large, r_h will monotonically increase with k . This explains the monotonically increasing behavior of HEE along k at a large k .

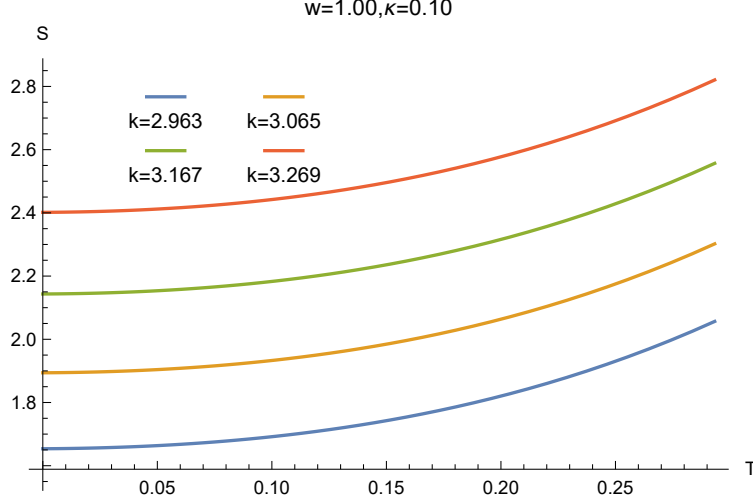


FIG. 7: The relation between HEE and T in the small configuration for model II. At other widths, HEE also increases monotonically with T .

Moreover, we also find that HEE increases monotonically with T , independent of the size of configuration and the values of κ , k and T (see Fig. 7). This phenomenon at high temperatures is understandable in an analytical manner. From (22) one finds that r_h is large when T is large. Varying the r_h and we can find,

$$\partial_T r_h = \frac{8\pi}{-\frac{8\kappa^{3/2}k^3}{J^3 r_h (r_h^2 + \kappa k^2)^2} + \frac{2\kappa k^2 (3r_h^2 + \kappa k^2)}{J^2 r_h^2 (r_h^2 + \kappa k^2)^2} + \frac{3k^4}{r_h^4} + 6}, \quad (26)$$

where $J \equiv \pi - 2 \arctan \left(\frac{r_h}{\sqrt{\kappa} k} \right)$. When r_h increases with T and becomes relatively large, J can be expanded as,

$$J = \frac{\pi}{2} - \frac{\sqrt{\kappa} k}{r_h} + O(r_h^{-2}). \quad (27)$$

Therefore, we find,

$$\begin{aligned} \partial_T r_h &= \frac{16\pi r_h^4 (r_h^2 + \kappa k^2)}{r_h^4 (12\kappa k^2 + 1) + 6k^4 r_h^2 + 12r_h^6 + 6\kappa k^6} \\ &= \frac{4\pi}{3} + O(1/r_h) > 0. \end{aligned} \quad (28)$$

From this relation, we find that HEE will increase with T . Also, when the temperature is relatively large, the slope of r_h vs T will be close to $4\pi/3$.

Next, we discuss the relationship between HEE and κ . HEE increases monotonically with κ for small configurations (see the left plot of Fig. 8); while for large configurations, HEE decreases monotonically with κ (see the right plot of Fig. 8). For large configurations, the

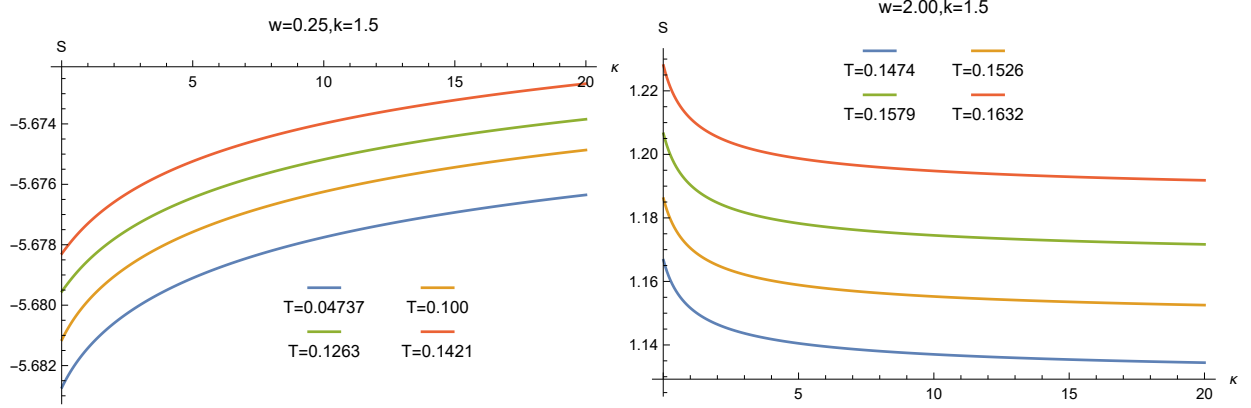


FIG. 8: The left and right graphs show the relationship between HEE and κ in the small and large configurations for model II respectively. It can be seen that HEE monotonically increases with κ in small configurations and decreases monotonically with κ in large configurations.

decreasing HEE along κ allows an analytical understanding when κ is small or large enough. First, when κ is small enough, we will find that,

$$\partial_{\kappa} r_h = -\frac{k^2 r_h}{3(12r_h^4 + r_h^2 + 6k^4)} + O(\kappa^1) < 0. \quad (29)$$

Therefore, r_h will decrease with the increase of κ , and HEE will also decrease with the increase of κ . Second, when κ is large, one finds that,

$$\partial_{\kappa} r_h = -\frac{r_h^5}{6\kappa^2 k^2 (2r_h^4 + k^4)} + O(\kappa^{-5/2}) < 0. \quad (30)$$

Therefore, again, we find that r_h decreases with κ when κ is large. Therefore, r_h will decrease with the increase of κ , and HEE will again decrease with the increase of κ .

In the case of intermediate configuration, the behavior of HEE with κ becomes complicated, which is related to the detailed values of the widths, k and T . The derivative of HEE with κ (Fig. 9) can clearly show the phenomena of intermediate configuration, which we expand in three cases.

1. When T is small, $S'(\kappa)$ is always positive, indicating that HEE increases monotonically with κ . This is consistent with the phenomenon in the left plot of Fig. 8.
2. When T gradually increases to a temperature around $T = 0.1158$, $S'(\kappa) < 0$ when κ is very small, but increases to be positive when κ is large. This indicates that HEE first decreases and then increases with κ .

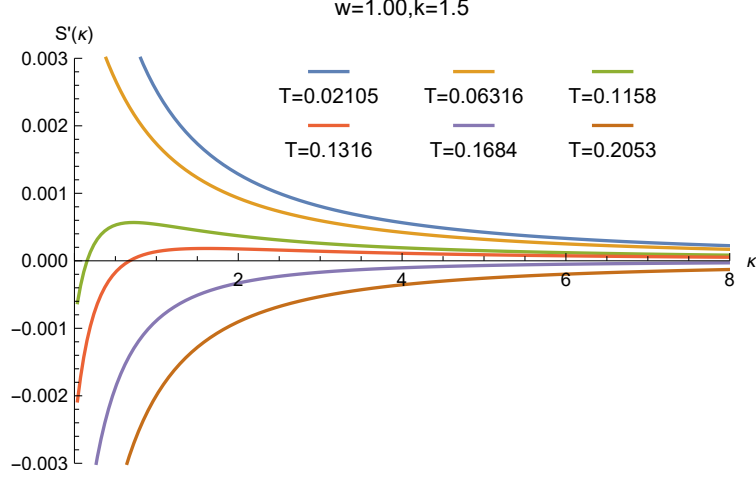


FIG. 9: The relationship between $\frac{\partial S}{\partial \kappa}$ and κ in one of the intermediate configurations for model II. It can be seen that at low temperature, HEE monotonically increased with κ , and with the increase of temperature, the behavior of HEE with κ decreased first and then increased, and with the further increase of temperature, HEE monotonically decreased with κ .

3. When T increases further, $S'(\kappa)$ is always negative, indicating that HEE decreases monotonically with κ . This is consistent with the phenomenon in the right plot of Fig. 8. In addition, a physical understanding is allowed here. With the increase of temperature, r_h will also increase. Therefore, the minimum surface of the intermediate configurations will also be close to the horizon of the black brane, so the relationship between HEE and κ will be the same as that of the large configuration.

C. Mutual information

For the configurations with nontrivial MI,

$$I(A; C) = S(A) + S(C) - S(B) - S(A \cup B \cup C). \quad (31)$$

Consequently, the derivative of MI with any system parameter x will be,

$$\frac{\partial I(A; C)}{\partial x} = \frac{\partial S(A)}{\partial x} + \frac{\partial S(C)}{\partial x} - \frac{\partial S(B)}{\partial x} - \frac{\partial S(A \cup B \cup C)}{\partial x}. \quad (32)$$

We find that $\frac{\partial S(B)}{\partial x} + \frac{\partial S(A \cup B \cup C)}{\partial x}$ is larger than $\frac{\partial S(A)}{\partial x} + \frac{\partial S(C)}{\partial x}$ in most cases. In other words, the change of the MI with parameters is mainly contributed by the part closer to horizon.

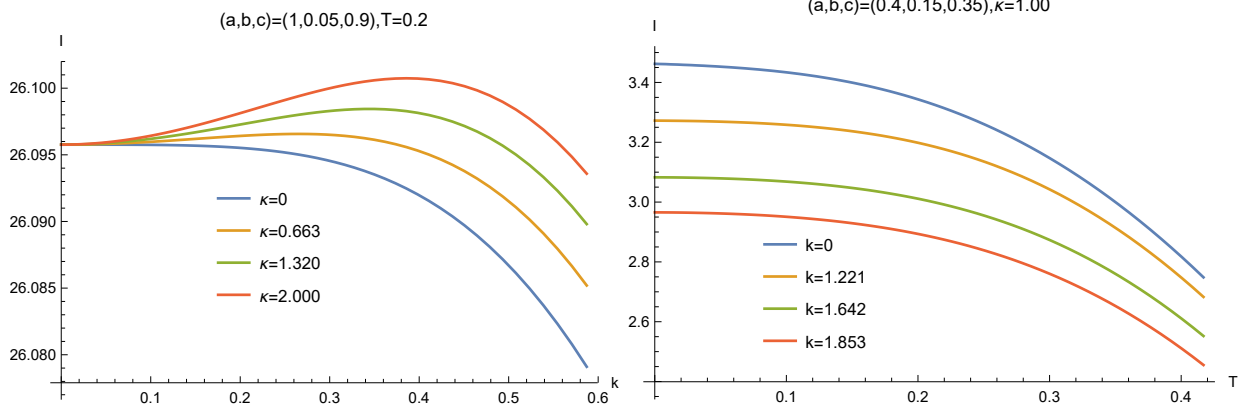


FIG. 10: The figure on the left shows the relationship between MI and k for model II. It can be seen that when κ is very small, MI decreases monotonically with k , and with the increase of κ , the behavior of MI increases first and then decreases with k . The figure on the right shows the relationship between MI and T for model II. It can be seen that MI decreases monotonically with T .

The reason is that the region closer to horizon is farther away from the boundary, so it is more affected by the deviation of AdS. Therefore, the change of MI with parameters will be completely opposite to that of HEE. Next we show numerical evidences.

MI decreases monotonically with k when the configuration and κ are not large. With the increase of configuration or κ , MI increases first and then decreases. We show this result as the left plot in Fig. 10. It is almost the opposite of the behavior shown in Fig. 6. Also, we find that MI decreases monotonically with T (see the right plot of Fig. 10), which is independent of the size of configuration and the values of κ , k and T . This is again opposite to HEE shown in Fig. 7. Finally, it can be inferred from the complicated relationship between HEE and κ that the relationship between MI and κ will also show a complicated but opposite relationship to HEE.

Next, we discuss the relationship between EWCS and system parameters in detail.

D. Entanglement Wedge Minimum Cross Section

First, we discuss the relationship between EWCS and k . The relationship between EWCS and k is related to the specific configuration, which we divide into the large configuration case and the small configuration case.

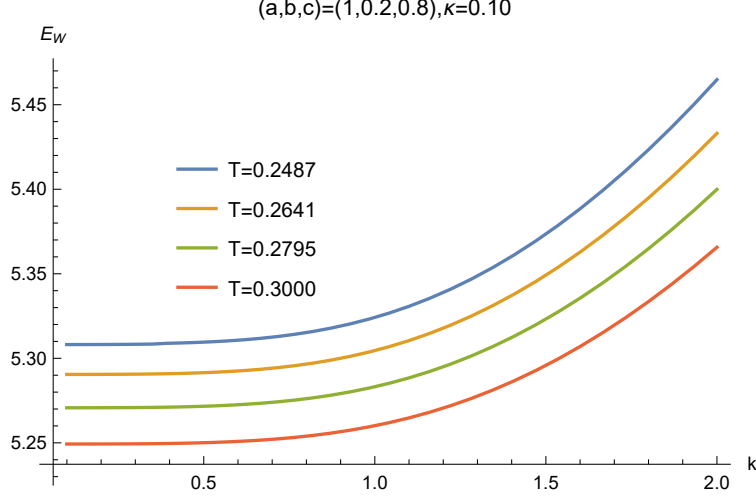


FIG. 11: The relation between EWCS and k in the large configuration for model II. It can be seen that EWCS increases monotonically with k , and has the same monotonic behavior with other large configurations and the values of T and κ .

1. For large configurations, EWCS increases monotonically with k , independent of the values of T and κ . We show this result in Fig. 11, and we also get the same conclusion in other large configurations.
2. For small configuration, EWCS exhibits rich phenomena with k . When the values of T and κ are appropriate, EWCS will decrease first and then increase with k (see Fig. 12). However, with the increase of T or κ , the decreasing behavior of EWCS with k becomes less significant, even disappears, and becomes monotonically increasing with k (see Fig. 13).

The above phenomena show that EWCS presents rich phenomena with k . It is particularly noteworthy that when k is large, EWCS always increases with the increase of k . Another obvious universal behavior is that when k is small, EWCS shows a flat behavior with k . These two common phenomena can be understood through an analytical treatment. Note that the EWCS is given by,

$$\begin{aligned}
 E_W &= \int \sqrt{g_{yy}} \sqrt{g_{xx} dx^2 + g_{rr} dr^2} \\
 &= \int r \sqrt{r^2 dx^2 + \frac{dr^2}{f(r)}}.
 \end{aligned} \tag{33}$$

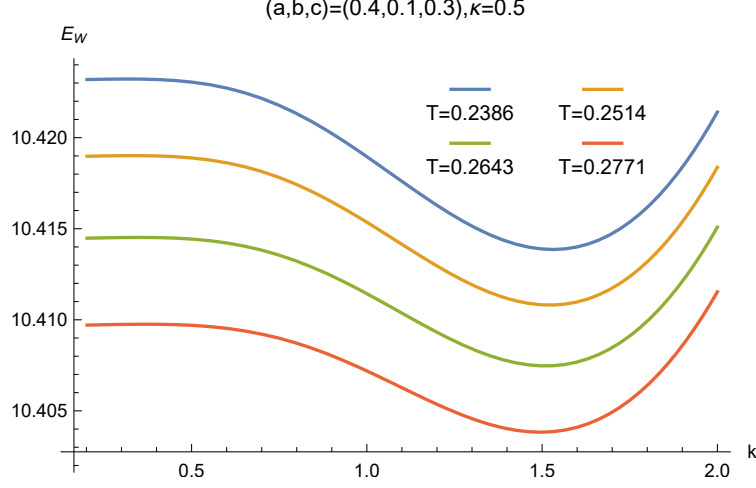


FIG. 12: The relation between EWCS and k in the small configuration for model II. It can be seen that when the values of T and κ are appropriate, EWCS first decreases and then increases with k .

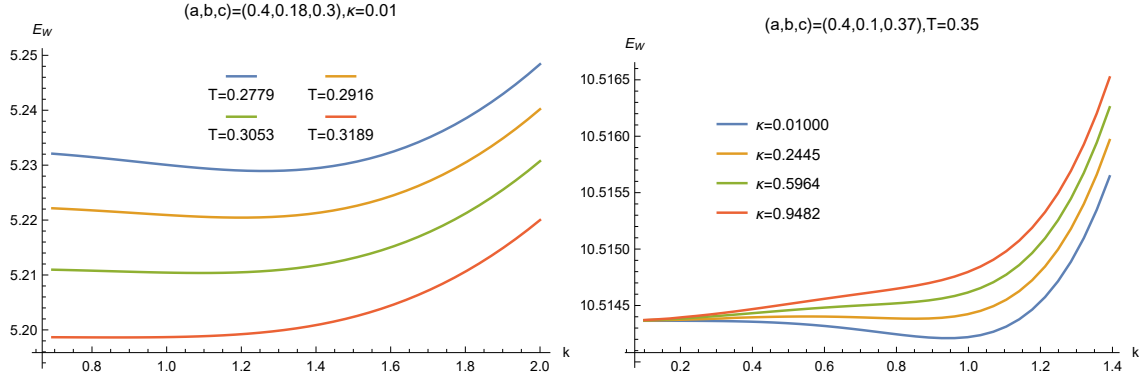


FIG. 13: The left and right figures show the relation between EWCS and k under different small configurations, T and κ for model II. It can be seen from the left figure that when T increases, the decreasing behavior of EWCS with k weakens or even disappears. It can be seen from the right figure that when κ increases, the decreasing behavior of EWCS with k weakens or even disappears.

Therefore, the E_W behavior with parameters depends on the $f(r)$.

$$\partial_\eta E_W = - \int \frac{r \partial_\eta f}{2f^2 \sqrt{\frac{dr^2}{f} + dx^2 r^2}} dr^2. \quad (34)$$

In large k -limit, we will find that

$${}_2F_1 \left(-\frac{1}{2}, 1; \frac{1}{2}; -\frac{r_h^2}{k^2 \kappa} \right) \rightarrow 1. \quad (35)$$

By working out $\partial_k r_h$ from (21), we can obtain that,

$$\partial_k f = \frac{2k^3 (3r_h - 2r)}{3r^2 r_h} + O(1/k). \quad (36)$$

Note that, the separation size b cannot be too large, otherwise the EWCS vanishes following from a vanishing MI. The E_W is mainly contributed from the region away from the near horizon region, i.e., $r \gg r_h$. Therefore, the main contribution to (34) from (36) will be positive. This relation explains the universal monotonically increasing behavior revealed in Fig. 11, 12 and 13. For relatively small k , one can also expand the $\partial_k f$ as,

$$\partial_k f = -\frac{\kappa k (-2r^2 r_h + r_h^3 + r^3)}{4r^4 r_h} + O(k^2). \quad (37)$$

It means that $\partial_k f \sim k$ for small k , which explains the flat behavior for E_W . However, whether the E_W increases or decreases with k depends on the specific configuration in consideration.

For the relationship between EWCS and T , we find that EWCS decreases monotonically with T , independent of the configuration, κ and k . We show this result in Fig. 14. This can be understood from the physical point of view that increasing the temperature will destroy the entanglement between the subregions. From the theory of quantum statistics, it can be understood that when the temperature of the system increases, the density matrix of the subsystem will be close to a product state of which each one is defined by the thermal density matrix. From the perspective of holographic duality, we can get a more vivid understanding. When the temperature increases, the minimum surface will approach the horizon of the black brane, so the HEE will be gradually controlled by the thermal entropy. When the temperature is very high, all the minimum surfaces will be contributed by the event horizon of the black brane, and MI is zero. Consequently, EWCS will vanish.

For the relationship between EWCS and κ , we find that EWCS increases monotonically with κ , and this behavior is independent of configuration, T and k . We show this result in Fig. 15. Further, it is noted that both HEE and MI showed non-monotonic behavior with κ . This shows that EWCS does reflect the different properties of mixed state entanglement of the system. When κ is large, E_W increases monotonically with κ and it becomes more and more flat. This flat behavior can also be analyzed analytically. Expanding $\partial_\kappa f$ around $1/\kappa \rightarrow 0$ gives,

$$\partial_\kappa f = \frac{r - r_h}{2\pi^2 \kappa r} + O(\kappa^{-3/2}). \quad (38)$$

Therefore, the $\partial_\kappa f$ becomes flat, which explains the flat behavior of E_W along κ .

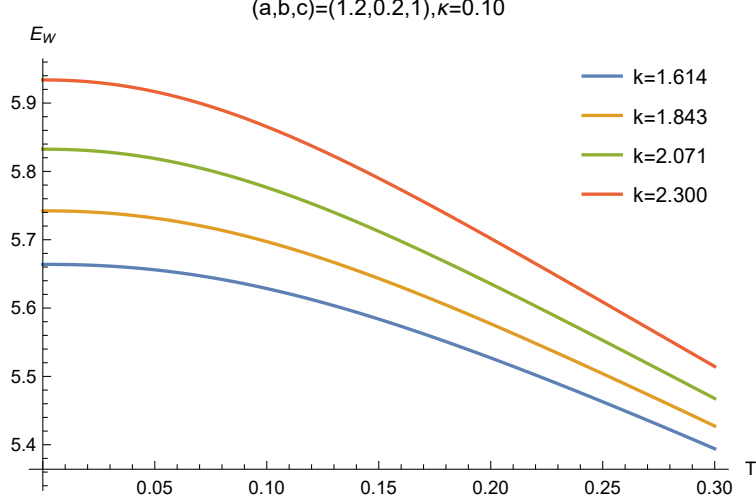


FIG. 14: The relation between EWCS and T for model II. It can be seen from the figure that EWCS decreases monotonically with T , and it also has the same monotonic behavior under other configurations, k and κ .

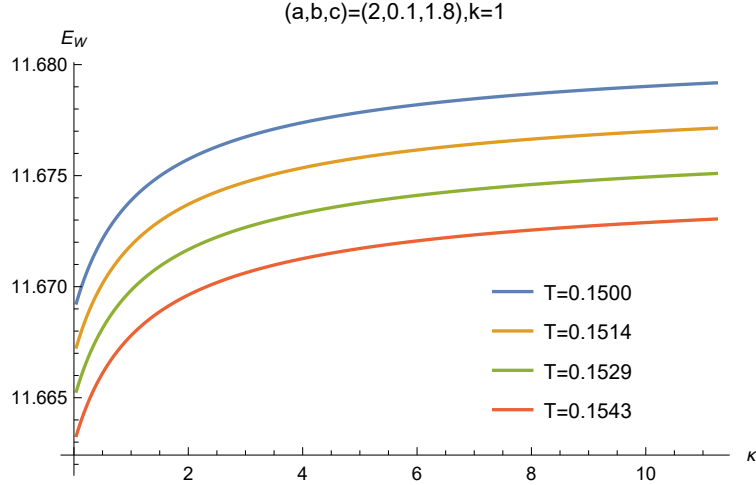


FIG. 15: The relation between EWCS and κ in model II. It can be seen from the figure that EWCS increases monotonically with κ , and it also has the same monotonic behavior under other configurations, k and T .

V. DISCUSSION

In this paper, we study the behavior of EWCS with system parameters of linear axion model I, and we also study the behavior of HEE and MI with three important parameters in the linear axion model II. In the exploration of model I, we find that the EWCS of asymmetric

configuration can show obvious non-monotonicity, which is an important supplement to the monotonicity of EWCS of previous symmetric configuration [51].

In model II, we find that the behavior of HEE and MI with three parameters are always opposite, which reflects the tight connection between HEE and MI. Moreover, we also found that HEE, MI and EWCS show monotonic behavior with temperature. In addition, we find that these information-related physical quantities show richer non-monotonic behavior with the linear axion parameter k . A more important phenomenon is that HEE and MI show non-monotonic behavior with the coupling constant κ , but EWCS shows monotonic behavior. These phenomena show that the mixed state entanglement EWCS captured is indeed distinct from the HEE and MI, those suffer from thermal entropy pollution. We also provide analytical and physical understanding of the above phenomena obtained from numerics.

Next, we point out several directions worthy of further study. First, the difference between EWCS and HEE and MI is worth studying in more general cases. For example, when $V(X) \neq X^2$, the conclusions in this paper are worth further testing and discussion. Second, we can further discuss the relationship between the measurement of entanglement of other types of mixed states and EWCS in this paper, such as negativity [58]. Finally, the analytical understanding in this paper can be further extended to more general parameter ranges, which will provide analytical evidence for the rich numerical results in this paper.

Acknowledgments

Peng Liu would like to thank Yun-Ha Zha for her kind encouragement during this work. This work is supported by the Natural Science Foundation of China under Grant No. 11805083, 11905083, 12005077 and Guangdong Basic and Applied Basic Research Foundation (2021A1515012374).

-
- [1] A. Donos and S. A. Hartnoll, “*Interaction-driven localization in holography*,” Nature Phys. **9**, 649 (2013)
 - [2] S. Ryu and T. Takayanagi, “*Holographic derivation of entanglement entropy from AdS/CFT*,” Phys. Rev. Lett. **96**, 181602 (2006)

- [3] L. Susskind, “*Computational Complexity and Black Hole Horizons*,” [Fortsch. Phys. **64**, 24 (2016)] Addendum: Fortsch. Phys. **64**, 44 (2016)
- [4] X. Dong, Nature Commun. **7**, 12472 (2016) [arXiv:1601.06788 [hep-th]].
- [5] A. Osterloh, L. Amico, G. Falci, R. Fazio, Nature **416**, 608 (2002) [arXiv:0202029 [quant-ph]]
- [6] L. Amico, R. Fazio, A. Osterloh and V. Vedral, Rev.Mod.Phys. **80**, 517 (2008) [arXiv:0703044 [quant-ph]]
- [7] Levin, Michael, and Xiao-Gang Wen. Physical review letters 96.11 (2006): 110405.
- [8] Kitaev, Alexei, and John Preskill. Physical review letters 96.11 (2006): 110404.
- [9] V. E. Hubeny, M. Rangamani and T. Takayanagi, JHEP **0707**, 062 (2007) [arXiv:0705.0016 [hep-th]].
- [10] A. Lewkowycz and J. Maldacena, JHEP **1308**, 090 (2013) [arXiv:1304.4926 [hep-th]].
- [11] X. Dong, A. Lewkowycz and M. Rangamani, JHEP **1611**, 028 (2016) [arXiv:1607.07506 [hep-th]].
- [12] Terhal, B.M., Horodecki, M., Leung, D.W. and DiVincenzo, D.P., 2002. Journal of Mathematical Physics, 43(9), pp.4286-4298.
- [13] Horodecki, R., Horodecki, P., Horodecki, M., Horodecki, K. (2009). Reviews of modern physics, 81(2), 865.
- [14] G. 't Hooft, “*Dimensional reduction in quantum gravity*,” Salamfest 1993:0284-296
- [15] L. Susskind, “*The World as a hologram*,” J. Math. Phys. **36**, 6377 (1995)
- [16] J. M. Maldacena, “*The Large N limit of superconformal field theories and supergravity*,” Int. J. Theor. Phys. **38**, 1113 (1999) [Adv. Theor. Math. Phys. **2**, 231 (1998)]
- [17] S. A. Hartnoll, “*Theory of universal incoherent metallic transport*,” Nature Phys. **11**, 54 (2015)
- [18] T. Nishioka and T. Takayanagi, JHEP **0701**, 090 (2007) [hep-th/0611035].
- [19] I. R. Klebanov, D. Kutasov and A. Murugan, Nucl. Phys. B **796**, 274 (2008) [arXiv:0709.2140 [hep-th]].
- [20] A. Pakman and A. Parnachev, JHEP **0807**, 097 (2008) [arXiv:0805.1891 [hep-th]].
- [21] S. J. Zhang, Nucl. Phys. B **916**, 304 (2017) [arXiv:1608.03072 [hep-th]].
- [22] X. X. Zeng and L. F. Li, Adv. High Energy Phys. **2016**, 6153435 (2016) [arXiv:1609.06535 [hep-th]].
- [23] Y. Ling, P. Liu, C. Niu, J. P. Wu and Z. Y. Xian, “*Holographic Entanglement Entropy Close to Quantum Phase Transitions*,” JHEP **1604**, 114 (2016)

- [24] Y. Ling, P. Liu and J. P. Wu, “Characterization of Quantum Phase Transition using Holographic Entanglement Entropy,” *Phys. Rev. D* **93**, no.12, 126004 (2016) doi:10.1103/PhysRevD.93.126004 [arXiv:1604.04857 [hep-th]].
- [25] S. H. Shenker and D. Stanford, *JHEP* **1403**, 067 (2014) [arXiv:1306.0622 [hep-th]].
- [26] Y. Sekino and L. Susskind, *JHEP* **0810**, 065 (2008) [arXiv:0808.2096 [hep-th]].
- [27] J. Maldacena, S. H. Shenker and D. Stanford, *JHEP* **1608**, 106 (2016) [arXiv:1503.01409 [hep-th]].
- [28] M. Blake, *Phys. Rev. Lett.* **117**, no. 9, 091601 (2016) [arXiv:1603.08510 [hep-th]].
- [29] M. Blake, *Phys. Rev. D* **94**, no. 8, 086014 (2016) [arXiv:1604.01754 [hep-th]].
- [30] Y. Ling, P. Liu and J. P. Wu, *JHEP* **1710**, 025 (2017) [arXiv:1610.02669 [hep-th]].
- [31] Y. Ling, P. Liu and J. P. Wu, *Phys. Lett. B* **768**, 288 (2017) [arXiv:1610.07146 [hep-th]].
- [32] S. F. Wu, B. Wang, X. H. Ge and Y. Tian, *Phys. Rev. D* **97**, no. 10, 106018 (2018) [arXiv:1702.08803 [hep-th]].
- [33] P. Liu, C. Niu and J. P. Wu, *Phys. Lett. B* **796**, 155 (2019) [arXiv:1905.06808 [hep-th]].
- [34] A. R. Brown, D. A. Roberts, L. Susskind, B. Swingle and Y. Zhao, *Phys. Rev. D* **93**, no. 8, 086006 (2016) [arXiv:1512.04993 [hep-th]].
- [35] A. R. Brown, D. A. Roberts, L. Susskind, B. Swingle and Y. Zhao, *Phys. Rev. Lett.* **116**, no. 19, 191301 (2016) [arXiv:1509.07876 [hep-th]].
- [36] S. Chapman, H. Marrochio and R. C. Myers, *JHEP* **1701**, 062 (2017) [arXiv:1610.08063 [hep-th]].
- [37] Y. Ling, Y. Liu and C. Y. Zhang, *Eur. Phys. J. C* **79**, no. 3, 194 (2019) [arXiv:1808.10169 [hep-th]].
- [38] B. Chen, W. M. Li, R. Q. Yang, C. Y. Zhang and S. J. Zhang, *JHEP* **1807**, 034 (2018) [arXiv:1803.06680 [hep-th]].
- [39] R. Q. Yang, H. S. Jeong, C. Niu and K. Y. Kim, *JHEP* **1904**, 146 (2019) [arXiv:1902.07586 [hep-th]].
- [40] Y. Ling, Y. Liu, C. Niu, Y. Xiao and C. Y. Zhang, *JHEP* **1911**, 039 (2019) [arXiv:1908.06432 [hep-th]].
- [41] J. Kudler-Flam, Y. Kusuki and S. Ryu, “Correlation measures and the entanglement wedge cross-section after quantum quenches in two-dimensional conformal field theories,” *JHEP* **04** (2020), 074 [arXiv:2001.05501 [hep-th]].

- [42] K. Babaei Velni, M. R. Mohammadi Mozaffar and M. H. Vahidinia, JHEP **08** (2020), 129 doi:10.1007/JHEP08(2020)129 [arXiv:2005.05673 [hep-th]].
- [43] M. Sahraei, M. J. Vasli, M. R. M. Mozaffar and K. B. Velni, JHEP **08** (2021), 038 doi:10.1007/JHEP08(2021)038 [arXiv:2105.12476 [hep-th]].
- [44] S. Khoeini-Moghaddam, F. Omid and C. Paul, “Aspects of Holographic Violating Geometries at Finite Cutoff,” JHEP **02** (2021), 121 doi:10.1007/JHEP02(2021)121 [arXiv:2011.00305 [hep-th]].
- [45] J. Kumar Basak, V. Malvimat, H. Parihar, B. Paul and G. Sengupta, [arXiv:2002.10272 [hep-th]].
- [46] K. Umemoto and T. Takayanagi, “*Entanglement of purification through holographic duality*,” Nature Phys. **14**, no. 6, 573 (2018)
- [47] K. Tamaoka, “Entanglement Wedge Cross Section from the Dual Density Matrix,” Phys. Rev. Lett. **122** (2019) no.14, 141601 [arXiv:1809.09109 [hep-th]].
- [48] P. Liu, C. Niu, Z. J. Shi and C. Y. Zhang, “*Entanglement Wedge Minimum cross section in Holographic Massive Gravity Theory*,” [arXiv:2104.08070 [hep-th]].
- [49] P. Liu, Y. Ling, C. Niu and J. P. Wu, Entanglement of Purification in Holographic Systems, JHEP **09**, 071 (2019) doi:10.1007/JHEP09(2019)071 [arXiv:1902.02243 [hep-th]].
- [50] Y. f. Huang, Z. j. Shi, C. Niu, C. y. Zhang and P. Liu, “*Mixed State Entanglement for Holographic Axion Model*,” Eur. Phys. J. C **80**, no.5, 426 (2020) doi:10.1140/epjc/s10052-020-7921-y [arXiv:1911.10977 [hep-th]].
- [51] P. Liu and J. P. Wu, “Mixed State Entanglement and Thermal Phase Transitions,” [arXiv:2009.01529 [hep-th]].
- [52] M. Baggioli and O. Pujolas, Phys. Rev. Lett. **114**, no. 25, 251602 (2015) doi:10.1103/PhysRevLett.114.251602 [arXiv:1411.1003 [hep-th]].
- [53] W. Fischler, A. Kundu and S. Kundu, Phys. Rev. D **87**, no.12, 126012 (2013) doi:10.1103/PhysRevD.87.126012 [arXiv:1212.4764 [hep-th]].
- [54] P. Chaturvedi, V. Malvimat and G. Sengupta, JHEP **05**, 172 (2018) doi:10.1007/JHEP05(2018)172 [arXiv:1609.06609 [hep-th]].
- [55] S. Dutta and T. Faulkner, JHEP **03**, 178 (2021) doi:10.1007/JHEP03(2021)178 [arXiv:1905.00577 [hep-th]].
- [56] L. Alberte, M. Baggioli, A. Khmelnitsky and O. Pujolas, JHEP **1602**, 114 (2016)

- doi:10.1007/JHEP02(2016)114 [arXiv:1510.09089 [hep-th]].
- [57] B. Goutéraux, E. Kiritsis and W. J. Li, JHEP **1604**, 122 (2016) [arXiv:1602.01067 [hep-th]].
- [58] J. Kudler-Flam and S. Ryu, Phys. Rev. D **99**, no.10, 106014 (2019)
doi:10.1103/PhysRevD.99.106014 [arXiv:1808.00446 [hep-th]].